HYDROGEN, FUEL CELL & ENERGY STORAGE

Facile hydrothermal synthesis and electrochemical investigation of a free-standing cobalt oxide hierarchical nanostructure electrode on a porous carbon structure as an efficient supercapacitor

G. Alaei | Mohammad Mazloum-Ardakani* | Fateme Ebrahimi

Department of Chemistry, Faculty of Science, Yazd University, P. O. Box 8915818411, Yazd, Iran
* Corresponding author, Email: mazloumardakani@gmail.com

Article Information

Article Type
Research Article

Article History
Received: *10 Mar 2024*
Revised: *15 May 2024*
Accepted: *01 Jun 2024*
Published Online: *05 Jun 2024*

Keywords

Cobalt oxide hierarchical nanostructure
Binder-free electrode fabrication
One-pot hydrothermal synthesis
Supercapacitor

Abstract

In the current work, we report the binder-free hydrothermal one-pot synthesis of a cobalt oxide hierarchical nanostructure (Co_3O_4-HNS) onto a highly conductive carbon fiber substrate (CFS/Co_3O_4-HNS) as an efficient electrode for energy storage devices. The fabricated electrode and synthesized Co_3O_4-HNS were structurally characterized using SEM, EDAX, XRD, and FTIR techniques. Electrochemical characterization of the fabricated CFS/Co_3O_4-HNS electrode was also performed and showed that the electrical double-layer capacitance and pseudo-capacitance mechanisms both play roles in the charge storage of the CFS/Co_3O_4-HNS electrode. The obtained results exhibited the electrochemical-specific capacitance of 715 F/g at a current density of 3 A/g for the CFE/Co_3O_4-HNS electrode. The fabricated electrode remains at 96% of its initial capacitance after 3000 cycles, showing the excellent cyclability of the fabricated CFS/Co_3O_4-HNS electrode. These results paved the way for using the proposed facile, one-pot synthesized CFE/Co_3O_4-HNS as an efficient electrode for use in electrochemical energy storage devices.

Cite this article: Alaei, G., Mazloum-Ardakani, M., Ebrahimi, F. (2024). Facile hydrothermal synthesis and electrochemical investigation of a free-standing cobalt oxide hierarchical nanostructure electrode on a porous carbon structure as an efficient supercapacitor. DOI: 10.22104/HFE.2024.6665.1285

 Publisher: Iranian Research Organization for Science and Technology (IROST)
DOI: 10.22104/HFE.2024.6665.1285

1 Introduction

The demand for powerful energy storage systems is rapidly increasing as the market for portable electronic devices and hybrid electric vehicles expands. This need has created a focus on high-performance energy storage devices with high energy density and rapid discharge capabilities [1–3]. Supercapacitors (SCs) have emerged as a promising solution due to advantages such as long cycling life, ease of fabrication, and high power density [4]. Based on their charge storage mechanism, SCs can be categorized into three types, including EDLCs or electric double-layer capacitors, pseudo-capacitors, and hybrid supercapacitors [5].

EDLCs store charges at the interface between the electrode and electrolyte through reversible ion adsorption from the electrolyte. Pseudo-capacitors, on the other hand, utilize the electron transfer at the electrode and electrolyte interface to store charges, leading to a greater specific capacitance than EDLCs [6]. Pseudo-capacitors commonly contain conducting polymers and/or transition metal oxides. Transition metal oxides show great potential for energy storage devices because of their high electrical conductivity, large surface area, theoretical specific capacitance, stability, abundance, and environmental friendliness [7].

Various oxides, such as MnO_2, IrO_2, RuO_2, Co_2O_3, V_2O_5, NiO, SnO_2, TiO_2, and Fe_2O_3, have been used to fabricate supercapacitor electrodes [8]. Cobalt oxide (Co_3O_4) has garnered significant attention due to its unique properties and potential applications in energy storage devices, catalysis, and electrochemical sensors [9, 10]. It offers high reversibility and controllable morphology, making it an attractive alternative to expensive materials like RuO_2.

Carbon-based materials composites have been fabricated to enhance the electroconductivity, rate performances, and specific capacitance of metal oxide electrodes, including amorphous carbon, graphene, carbon nanofibers, and carbon nanotubes [11, 12]. In this study, we employed the hydrothermal synthesis method to direct binder-free cobalt oxide hierarchical nanostructures (Co_3O_4-HNS) onto a carbon fiber electrode (CFS/Co_3O_4-HNS) without the need for binders. This method paved the way for the one-pot, facile synthesis of CFS/Co_3O_4-HNS free-standing electrodes for high-performance, efficient supercapacitors.

2 Experimental

2.1 Materials

Reagent-grade potassium hydroxide (KOH), Urea ($CO(NH_2)_2$), ammonium fluoride (NH_4F), cobalt nitrate hexahydrate ($Co(NO_3)_2 \cdot 6\,H_2O$) were available from Sigma-Aldrich company and were used without further purification.

2.2 One-pot hydrothermal synthesis of the Co_3O_4-HNS arrays on carbon fiber electrode (CF/Co_3O_4-HNS)

To prepare the CF/Co_3O_4-HNS electrode, the carbon substrate was first thoroughly washed several times using di-ionized water. Then, the Co_3O_4-HNS arrays were synthesized on a carbon fiber electrode through a hydrothermal reaction and subsequent calcination process. For this purpose, a volume of 50 mL solution containing NH_4F, $CO(NH_2)_2$, and $Co(NO_3)_2 \cdot 6\,H_2O$ (0.148 g, 0.6 g, and 0.29 g, respectively) was prepared in deionized water and stirred for 30 minutes creating a homogeneous purple solution. Next, the solution and carbon fiber substrate were put into a Teflon-lined stainless steel autoclave (hydrothermal reactor) and tightly sealed. The hydrothermal reactor was then kept at a temperature of 120 °C for five hours. Afterward, the resulting electrodes were rinsed multiple times with DI water and ethanol and dried for 12 h at 60 °C. Finally, the obtained electrodes were heated at 350 °C for 150 minutes, using a 2 °C/min ramping rate, resulting in the fabrication of the CF/Co_3O_4-HNS electrode [13].

2.3 Characterization methods

A field-emission scanning electron microscope (SEM, Mira(III) XMU, TESCAN Company) was utilized to examine the surface morphology of both the bare CF electrode and the CF/Co_3O_4-HNS electrodes. In order to determine the composition and phase of the Co_3O_4-HNS, X-ray diffraction (XRD) measurements were taken using a Bruker D8 Advance (Germany) diffractometer. A Fourier transform infrared spectrometer (FTIR, Bruker Equinox 55 single beam spectrometer) was employed to identify the functional groups present in the synthesized materials.

2.4 Electrochemical characterization

An electrochemical Zieve lab workstation (SP2 model, Korea) was utilized to conduct all electrochemical measurements at room temperature. The electrochemical performance analysis of the samples was carried out using a conventional three-electrode system with a 3 mol/L KOH electrolyte solution. A platinum wire was employed as the auxiliary, a saturated calomel electrode (SCE) as the reference, and the CF/Co_3O_4-HNS

electrode as the working electrode. Cyclic voltammetry (CV) studies were performed within 0.0-0.4 V to assess the electrochemical performance of the CF/Co_3O_4-HNS electrode at various scan rates. Galvanostatic charge-discharge (GCD) was performed for different current densities, in 0-0.4 V (vs. SCE).

Electrochemical impedance spectroscopy (EIS) was performed across the 100 kHz to 1 Hz frequency range, with 10 mV alternative current oscillation. The discharge curves specific capacitance (C_{sp}) was calculated using the following equation [13,14]:

$$C_{sp} = \frac{It}{\Delta V\, m}\,, \tag{1}$$

where I represents the current of the discharge cycle (A), t is the time of the discharge cycle (s), ΔV denotes potential range (V), and m signifies the active material's mass (g).

3 Results and discussion

3.1 Fabrication and structural characterization of CF/Co_3O_4-HNS electrode

The CF/Co_3O_4-HNS electrode was fabricated through one-step binder-free hydrothermal synthesis followed by calcination. The hydrothermal reactions involved the attachment of $Co_2(OH)_2CO_3$ arrays onto the carbon fiber surface. Within this reaction, the interaction between Co^{2+} and F led to the formation of an intermediate product known as $CoF_a{}^{(a-2)-}$ [13]. Simultaneously, urea, when dissolved in water, contributed carbonate and hydroxyl anions. Subsequently, the $CoF_a{}^{(a-2)-}$ species reacted with $CO_3{}^{2-}$ and OH^- to generate cobalt hydroxide carbonate species. Notably, the self-assembly of the nanostructure is crucially affected and facilitated by the inclusion of NH4F molecules in the activation process [13,15]. Finally, the calcination process was performed under an air atmosphere at 350 °C, resulting in the formation of porous Co_3O_4 hierarchical nanostructure arrays. The following equations describe these reactions [16,17]:

$$Co^{2+} + aF^- \longrightarrow CoF_a{}^{(a-2)-}\,, \tag{2}$$

$$Co(NH_2)_2 + H_2O \longrightarrow 2\,NH_3 + CO_2\,, \tag{3}$$

$$CO_2 + H_2O \longrightarrow CO_2{}^{3-} + 2\,H^+\,, \tag{4}$$

$$2\,CoF_a{}^{(a-2)-} + 2\,OH^- + CO_2{}^{3-} + nH_2O \longrightarrow Co_2(OH)_2CO_3 \cdot nH_2O + 2aF^-\,, \tag{5}$$

$$3\,Co_2(OH)_2CO_3 \cdot nH_2O + O_2 \longrightarrow 3\,CO_2 + 3(n+1)H_2O + 3\,Co_3O_4\,. \tag{6}$$

SEM analysis was employed to examine the morphologies of bare CFS and CFS/Co_3O_4-HNS electrodes. Figure 1a illustrates the SEM images of the CFS, which exhibits a 3D porous structure with relatively smooth surfaces on each carbon fiber. This 3D structure offers a larger surface area, facilitating the growth of more active materials. The SEM images of the CFS/Co_3O_4-HNS electrode (Figure 1b) reveal a uniform distribution of hierarchical nanostructures containing hexagonal plates at the outer layer and an underlying layer composed of an ultra-thin nanosheet porous structure.

X-ray diffraction is a widely employed method to analyze the crystalline structure and composition of a given sample. This technique utilizes X-ray beams because their wavelength is comparable to the spacing between atoms in the sample. Consequently, the angle of diffraction is influenced by the arrangement of atoms within the molecule, as opposed to longer wavelengths that remain unaffected by atomic spacing. The X-rays penetrate the sample, interacting with the atoms in the structure and altering the direction of the beam at a distinct angle, known as theta, in relation to the original beam. While some of these diffracted beams cancel each other out, constructive interference occurs when the beams possess similar wavelengths. By applying Bragg's law, the angle of diffraction can be utilized to determine the disparity between atomic planes. Consequently, the distance between atomic planes can be employed to ascertain the crystalline structure or composition of the sample.

The XRD technique was utilized to verify the phase composition and crystallinity of the as-prepared Co_3O_4-HNS. As can be seen from Figure 1c, the XRD spectrum's peaks (2θ = 19.0 (111), 31.2 (220), 36.9 (311), 38.5 (222), 44.8 (400), 55.6 (422), 59.3 (511) and 65.1 (440)) are in good agreement with the JCPDS card [JCPDS040850] [18].

Figure 1d shows the FTIR spectrum of Co_3O_4-HNS in the wavenumber range of 400 to 4000 cm^{-1}. The broad band at 3429 cm^{-1} is due to the stretching vibration mode of O−H groups. The peaks at 2923 and 2854 cm^{-1} correspond to the asymmetric and symmetric stretching of the C−H band, respectively; the doublet at 2360 cm^{-1} represents the absorption by CO_2. The peak at 1637 cm^{-1} belongs to the C−O bend from carbon impurities, and peaks at 1440 and 1394 cm^{-1} are related to the CH_2 and CH_3 deformation and the stretching vibration of $NO_3{}^-$, respectively. Peaks at 1035 and 905 cm^{-1} are related to the C−N deformation and N−H vibrations [19]. These peaks are due to the residue of NH_4F, urea, and $Co(NO_3)_3$ residues, which provide functional groups that improve the electrostatic adsorption of ions onto the synthesized nanoma-

terial structure. The absorption band at 572 cm^{-1} and 667 cm^{-1} was assigned to the Co−O stretching vibration mode and the bridging vibration of the O−Co−O bond, respectively [20].

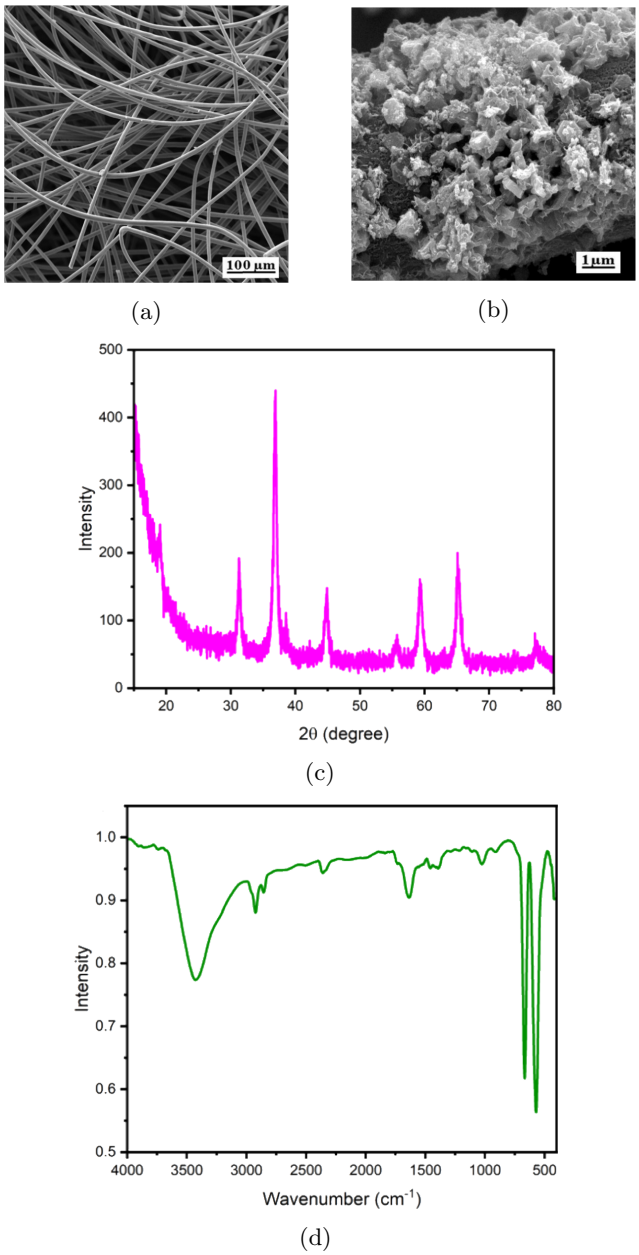

Fig. 1. SEM images of (a) CFS and (b) CFS/Co_3O_4-HNS), (c) XRD pattern, and (d) FTIR spectrum of hydrothermally, one-pot synthesized Co_3O_4-HNS.

3.2 Electrochemical characterization of CFS/Co_3O_4-HNS electrode

To evaluate the electrochemical performance of the CFS/Co_3O_4-HNS electrode, cyclic voltammetry (CV), galvanostatic charge-discharge (GCD), and impedance measurements were conducted [21]. The evaluations were performed in 3 mol/L KOH using a conventional three-electrode electrochemical setup.

Figure 2a demonstrates the CV of the CFS/Co_3O_4-HNS electrode at different potential windows from 0 to 0.65 V. Various oxidation states of the cobalt ions in the highly alkaline electrolyte caused pseudocapacitance behavior of the electrode via different peak situations on the cyclic voltammogram. The relatively wide peak in the potential region from 0.35 to 0.6 V is due to Co(II) and Co(III) oxidation. The two peaks with the minimum at 0.22 and 0.13 in the reverse scan are related to the Co(IV) and Co(III) reduction, respectively. The overall shape of cyclic voltammograms is highly dependent on surface characteristics, such as functional groups present at the surface, morphology, and the intrinsic properties of the matter. Here, during the oxidation step in the anodic scan, $Co(OH)_2$ species were generated from the reduced Co_3O_4 produced in the cathodic scan [22–25].

Here, the potential window was selected so that the oxidation reactions occurred partially. This rational selection of the potential window (from 0 to 0.4 V) causes partial oxidation of the cobalt, minimizing the structural changes of the electrode's nanostructure after successive cycling experiments. This strategy provides an extremely long lifespan for the fabricated CFS/Co_3O_4-HNS electrode.

Figure 2b shows the characteristic cyclic voltammograms observed for the bare CFS and CFS/Co_3O_4-HNS electrodes. These voltammograms were obtained using a scan rate of 0.1 V/s, within a potential range of 0 to 0.4 V. In the case of the bare CFS electrode, the cyclic voltammogram exhibits capacitive behavior primarily attributed to the electrochemical double-layer capacitance (EDLC) mechanism for charge storage. However, following the growth of Co_3O_4-HNS, the cyclic voltammogram demonstrates capacitive behavior primarily arising from both EDLC and faradaic reactions involving the $Co^{2+}/Co^{3+}/Co^{4+}$ redox couples in conjunction with Na^+ and OH^- ions [22].

The response current and enclosed area of the CFS/Co_3O_4-HNS electrode are compared to that of the bare CFS electrode, revealing a significant increase. This suggests that the CFS/Co_3O_4-HNS electrode exhibits more pronounced capacitive properties and enhanced electrochemical reaction activity. CV tests were conducted at various scan rates to assess the electrode's long-term cycling stability and rate capability. The obtained CV curves at various scan rates (ranging from 20 to 80 mV/s) for the CFS/Co_3O_4-HNS electrode are shown in Figure 2c. It is worth noting that the overall shape of the CV curves remains relatively consistent as the scan rate increases. These findings suggest

that the interface between the electroactive material and the electrolyte exhibits exceptional rate capability, demonstrating excellent ionic and electronic transportation [26].

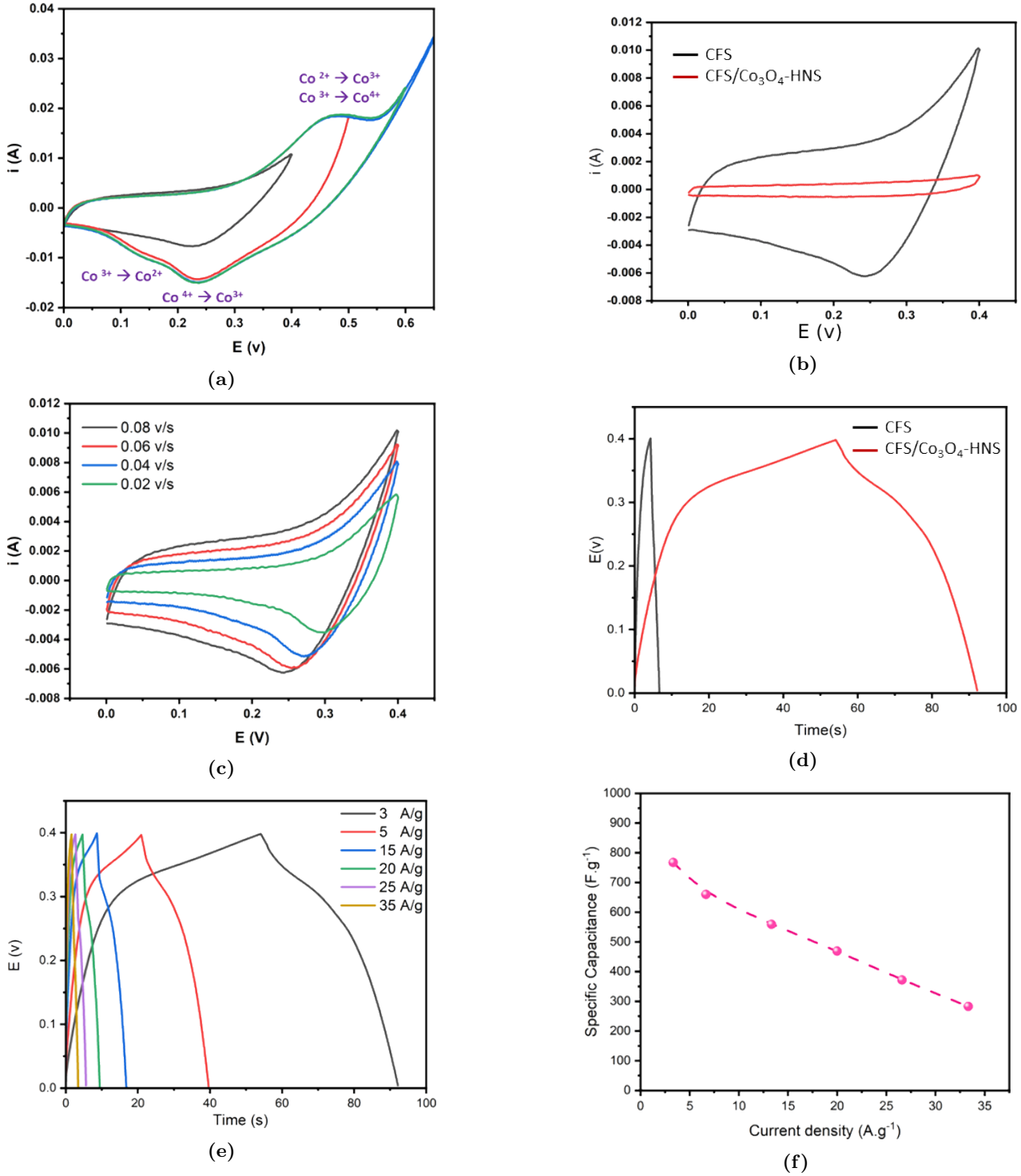

Fig. 2. (a) Cyclic voltammogram of the fabricated CFS/Co_3O_4-HNS electrode serving Ag/AgCl and Pt as reference and counter electrodes, respectively, in different potential windows from 0 to 0.4, 0.5, 0.6, and 0.65 volts in KOH 6M, (b) overlay of the cyclic voltammogram of the bare CFS and CFS/Co_3O_4-HNS electrodes, (c) cyclic voltammograms of the CFS/Co_3O_4-HNS electrode at different scan rates, (d) GCD of the CFS and CFS/Co_3O_4-HNS electrodes, (e) GCD of the CFS/Co_3O_4-HNS electrode at different current densities, (f) the correlation of current densities and specific capacitances of the samples.

Figure 2d illustrates the galvanostatic charge/discharge (GCD) curves of the bare CFS and CFS/Co_3O_4-HNS electrodes, measured within 0 to 0.4 V at 3 A/g. The GCDs exhibit characteristic pseudo-capacitance behavior consistent with the obtained cyclic voltammograms. Notably, the CFS/Co_3O_4-HNS discharge time was determined to be 92.135 s, surpassing the 6.61 s discharge time of the bare CFS electrode. The specific capacitance of CFS/Co_3O_4-HNS was determined to be 715 F/g based on Equation (2) and discharge information. The enhanced electrochemical characteristics of the CFS/Co_3O_4-HNS electrode can be ascribed to its increased surface area, which affords increased transmission channels and active sites for ion/electron transfer and storage. GCD tests were performed on the CFS/Co_3O_4-HNS within 3 to 35 A/g and 0.0 to 0.4 V to evaluate the electrodes' long-term cycling stability, rate capability, and specific capacitance. Figure 2e shows the GCD curves of the CFS/Co_3O_4-HNS electrode at various current densities, indicating a gradual decrease in discharge time as the current density increased [27, 28].

Figure 2f illustrates the correlation of current densities and specific capacitances of the samples. It is important to highlight that the CFS/Co_3O_4-HNS electrode maintains approximately 61% of its initial capacitance by increasing the current densities up to 20 A/g, demonstrating its excellent rate capability. The significant specific capacitance value of the CFS/Co_3O_4-HNS electrode can be attributed to two factors: the hierarchical nanostructure array of Co_3O_4 nanostructures on the CFS electrode and the pseudo-capacitance mechanism resulting from various oxidation states of the fabricated Co_3O_4-HNS. These factors contribute to the creation of numerous active sites for redox reactions and enable the formation of effective channels for the diffusion of electrolyte ions [29].

Furthermore, an investigation was conducted by performing 3000 GCD cycles at a current density of 6 A/g in a 3 mol/L KOH electrolyte to assess the durability over extended cycling periods, a crucial aspect for the application of electrochemical capacitors. Remarkably, even after 3000 consecutive cycles, the CFS/Co_3O_4-HNS electrode retained 97% of its initial capacitance, indicating the exceptional cycle ability of the fabricated electrode through rational selection of the potential window, which provides partial oxidation of the electrode surface in each cycle [30].

The changes in the CFS/Co_3O_4-HNS electrode surface caused by the modification process were monitored using electrochemical impedance spectroscopy (EIS). EIS analysis was conducted in a 3 mol/L KOH electrolyte at the open circuit potential (OCP) across a frequency range of 100 kHz to 1 Hz. The impedance spectroscopy data showed distinctive features comprising curved and straight segments. The curved portion represents the electron transfer dynamics, with its diameter reflecting the electron transfer resistance (R_{ct}) and providing insights into electron transfer kinetics at the electrode interface. On the other hand, the intersection of the real axis in the high-frequency region designates the electrochemical system's resistance (R_s), which encompasses contact resistance, electrolyte resistance, and electroactive material resistance. Lastly, the straight section observed at lower frequencies is related to diffusion [22, 31].

Figure 3 compares the Nyquist plots of the unmodified CFS electrode and the CFS/Co_3O_4-HNS electrode. Small semicircles in higher frequencies for both electrodes exhibit negligible charge transfer resistance and efficient electron transfer kinetics at the interface between the electrode and electrolyte. Furthermore, the straight line's slope in the low-frequency region can be ascribed to the electrode's capacitive properties [13,32]. After the Co_3O_4-HNS grows on the electrode surface, Rct increases because of the addition of a new layer of porous metal oxide at the electrode/electrolyte interface. However, the charge transfer resistance in both CFS and CFS/Co_3O_4-HNS is very low, which does not interfere with the charge transfer at the electrode/electrolyte interface and the charge storage mechanism of the electrode. These results show the good potential of the fabricated CFS/Co_3O_4-HNS electrode for high-performance supercapacitor fabrication.

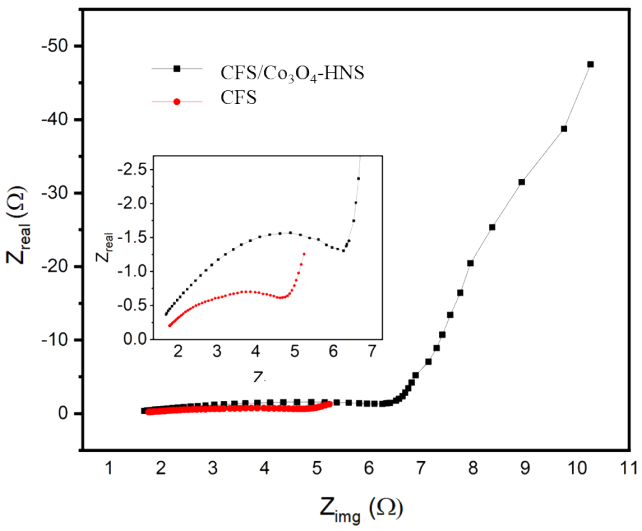

Fig. 3. Nyquist plot for bare CFS and CFS/Co_3O_4-HNS electrodes recorded at the open circuit potential in the KOH 6M and the frequency range from 100 kHz to 1 Hz, serving Ag/AgCl, Pt, and CFS/Co_3O_4-HNS as reference, counter and working electrodes.

4 Conclusions

In this study, a hierarchical nanostructure porous tricobalt tetra-oxide array modified carbon fiber substrate was successfully fabricated using a facile, binder-free, one-step hydrothermal synthesis method followed by subsequent calcination. The resulting electrode was characterized through XRD, SEM, EDX, and FTIR analysis. The capacitance behavior of the CFS/Co_3O_4-HNS electrode was investigated electrochemically through CV, GCD, and EIS experiments. The CFS/Co_3O_4-HNS electrode exhibited remarkable pseudocapacitive performance, demonstrating a high specific capacitance of 715 F/g at the current density of 3 A/g, along with excellent cycling stability of 97% after 3000 cycles. This enhanced supercapacitive performance can be attributed to three main factors. Firstly, it stems from the well-defined porous structure of the CF substrate, along with well-shaped hierarchical nanostructures of the hydrothermally grown cobalt oxide array, which provides suitable holes and porosity for ion transportation and storage. Second, it is related to the partial oxidation of the prepared nanostructure during the calcination process, making the surface more desirable for ion adsorption/desorption by providing suitable functional groups, and third, it arises from the intrinsic capacitance properties of the cobalt oxide compound, which provides different oxidation states accompanying in the charge storage through the pseudo-capacitance mechanism and rational selection of the potential window to provide a partial surface oxidation state. The fabricated CFS/Co_3O_4-HNS electrode maintains 61% of its initial capacitance at current densities as high as 20 A/g. The obtained results highlight the considerable potential of the synthesized CFS/Co_3O_4-HNS electrode for practical applications in the development of supercapacitors.

Acknowledgments

The authors wish to thank the Yazd University Research Council for financially supporting this research.

References

[1] Babu RS, Vinodh R, De Barros A, Samyn L, Prasanna K, Maier M, et al. Asymmetric supercapacitor based on carbon nanofibers as the anode and two-dimensional copper cobalt oxide nanosheets as the cathode. Chemical Engineering Journal. 2019;366:390–403.

[2] Wang X, Hu A, Meng C, Wu C, Yang S, Hong X. Recent advance in Co_3O_4 and Co_3O_4-containing electrode materials for high-performance supercapacitors. Molecules. 2020;25(2):269.

[3] Gür TM. Review of electrical energy storage technologies, materials and systems: challenges and prospects for large-scale grid storage. Energy & Environmental Science. 2018;11(10):2696–2767.

[4] Raghavendra KVG, Vinoth R, Zeb K, Gopi CVM, Sambasivam S, Kummara MR, et al. An intuitive review of supercapacitors with recent progress and novel device applications. Journal of energy storage. 2020;31:101652.

[5] Jalal NI, Ibrahim RI, Oudah MK. A review on Supercapacitors: Types and components. In: Journal of Physics: Conference Series. vol. 1973. IOP Publishing; 2021. p. 012015.

[6] Fleischmann S, Zhang Y, Wang X, Cummings PT, Wu J, Simon P, et al. Continuous transition from double-layer to Faradaic charge storage in confined electrolytes. Nature Energy. 2022;7(3):222–228.

[7] Ma Y, Xie X, Yang W, Yu Z, Sun X, Zhang Y, et al. Recent advances in transition metal oxides with different dimensions as electrodes for high-performance supercapacitors. Advanced Composites and Hybrid Materials. 2021;p. 1–19.

[8] Alshoaibi A, Awada C, Alnaim N, Almulhem N, Obodo RM, Maaza M, et al. Investigation of chemical bath deposited transition metals/GO nanocomposites for supercapacitive electrodes. Crystals. 2022;12(11):1613.

[9] Velhal NB, Yun TH, Ahn J, Kim T, Kim J, Yim C. Tailoring cobalt oxide nanostructures for stable and high-performance energy storage applications. Ceramics International. 2023;49(3):4889–4897.

[10] Benchettara A, Benchettara A. Electrochemical sensor based on nanoparticles of cobalt oxides for determination of glucose. Materials Today: Proceedings. 2015;2(8):4212–4216.

[11] Dubey R, Guruviah V. Review of carbon-based electrode materials for supercapacitor energy storage. Ionics. 2019;25:1419–1445.

[12] Lakra R, Kumar R, Sahoo PK, Thatoi D, Soam A. A mini-review: Graphene based composites for supercapacitor application. Inorganic Chemistry Communications. 2021;133:108929.

[13] Sanayee M, Arvand M. Characterization of Co-Mn layered double hydroxide nanostructures covered on Co_3O_4 as electrode material for supercapacitor applications. Solid State Ionics. 2022;383:115993.

[14] Lakra R, Kumar R, Thatoi DN, Sahoo PK, Soam A. Synthesis and characterization of cobalt oxide (Co_3O_4) nanoparticles. Materials Today: Proceedings. 2021;41:269–271.

[15] Wang Y, Lei Y, Li J, Gu L, Yuan H, Xiao D. Synthesis of 3D-nanonet hollow structured Co_3O_4 for high capacity supercapacitor. ACS applied materials & interfaces. 2014;6(9):6739–6747.

[16] Jiang J, Liu J, Huang X, Li Y, Ding R, Ji X, et al. General synthesis of large-scale arrays of one-dimensional nanostructured Co_3O_4 directly on heterogeneous substrates. Crystal growth & design. 2010;10(1):70–75.

[17] Wang X, Fu J, Wang Q, Dong Z, Wang X, Hu A, et al. Preparation and electrochemical properties of Co_3O_4 supercapacitor electrode materials. Crystals. 2020;10(9):720.

[18] Lu Y, Zhan W, He Y, Wang Y, Kong X, Kuang Q, et al. MOF-templated synthesis of porous Co_3O_4 concave nanocubes with high specific surface area and their gas sensing properties. ACS applied materials & interfaces. 2014;6(6):4186–4195.

[19] Rabee AI, Gaid CB, Mekhemer GA, Zaki MI. Combined TPR, XRD, and FTIR studies on the reduction behavior of Co_3O_4. Materials Chemistry and Physics. 2022;289:126367.

[20] Ai LH, Jiang J. Rapid synthesis of nanocrystalline Co_3O_4 by a microwave-assisted combustion method. Powder Technology. 2009;195(1):11–14.

[21] Xu J, Gao L, Cao J, Wang W, Chen Z. Preparation and electrochemical capacitance of cobalt oxide (Co_3O_4) nanotubes as supercapacitor material. Electrochimica Acta. 2010;56(2):732–736.

[22] Meher SK, Rao GR. Ultralayered Co_3O_4 for high-performance supercapacitor applications. The Journal of Physical Chemistry C. 2011;115(31):15646–15654.

[23] Xiong S, Yuan C, Zhang X, Xi B, Qian Y. Controllable synthesis of mesoporous Co_3O_4 nanostructures with tunable morphology for application in supercapacitors. Chemistry–A European Journal. 2009;15(21):5320–5326.

[24] Yang Q, Lu Z, Sun X, Liu J. Ultrathin Co_3O_4 nanosheet arrays with high supercapacitive performance. Scientific Reports. 2013;3(1):3537.

[25] Yan AL, Wang XC, Cheng JP. Research progress of NiMn layered double hydroxides for supercapacitors: A review. Nanomaterials. 2018;8(10):747.

[26] Wang X, Li M, Chang Z, Yang Y, Wu Y, Liu X. Co_3O_4@ MWCNT nanocable as cathode with superior electrochemical performance for supercapacitors. ACS applied materials & interfaces. 2015;7(4):2280–2285.

[27] Pan X, Chen X, Li Y, Yu Z. Facile synthesis of Co_3O_4 nanosheets electrode with ultrahigh specific capacitance for electrochemical supercapacitors. Electrochimica Acta. 2015;182:1101–1106.

[28] Ali F, Khalid NR, Nabi G, Ul-Hamid A, Ikram M. Hydrothermal synthesis of cerium-doped Co_3O_4 nanoflakes as electrode for supercapacitor application. International Journal of Energy Research. 2021;45(2):1999–2010.

[29] Pal M, Rakshit R, Singh AK, Mandal K. Ultra high supercapacitance of ultra small Co_3O_4 nanocubes. Energy. 2016;103:481–486.

[30] Kwak JH, Lee YW, Bang JH. Supercapacitor electrode with an ultrahigh Co_3O_4 loading for a high areal capacitance. Materials letters. 2013;110:237–240.

[31] Meher SK, Rao GR. Effect of microwave on the nanowire morphology, optical, magnetic, and pseudocapacitance behavior of Co_3O_4. The Journal of Physical Chemistry C. 2011;115(51):25543–25556.

[32] Wei TY, Chen CH, Chang KH, Lu SY, Hu CC. Cobalt oxide aerogels of ideal supercapacitive properties prepared with an epoxide synthetic route. Chemistry of Materials. 2009;21(14):3228–3233.